Aust. J. Phys., 1983, **36**, 135–53

An Analytic Distorted Wave Approximation for Intermediate Energy Proton Scattering

F. Di Marzio and K. Amos

School of Physics, University of Melbourne,
Parkville, Vic. 3052.

Abstract

An analytic distorted wave approximation (ADWA) has been developed for use in analyses of intermediate energy inelastic proton scattering from nuclei. Applications are made to analyse 402 and 800 MeV data from the isoscalar and isovector 1^+ and 2^+ states in ^{12}C and to the 800 MeV data from the excitation of the 2^-(8·88 MeV) state in ^{16}O. Comparisons of predictions made using different model two-nucleon t matrices and different models of nuclear structure are given.

1. Introduction

It has long been realized that nuclear reaction data initiated by nucleons with energies less than 100 MeV were of limited use in determining properties of nuclear structure. Not only was the nuclear structure content of the reaction analyses diffused by folding with a two-nucleon t matrix whose characteristics were largely unknown, but also distortion effects in the entrance and exit channel functions were significant and necessary to successfully predict data. Furthermore, analyses of selected transitions for which nuclear spectroscopy was well understood provided information about the two-nucleon t matrix, but only for a small range of low momentum transfers (0 to 2 fm^{-1} typically). Consequently there has been much interest in intermediate energy (>100 MeV) data, because not only are distortion effects in analyses less severe than for low energy reactions, but also data can be obtained at higher values of momentum transfer. Furthermore, simplifying approximation techniques, such as the impulse approximation, are expected to be of use with increasing projectile energies and the nuclear two-nucleon t matrices should not be far removed, if at all, from those of two nucleons. Even so, a variety of model t matrices has been promulgated in the literature and the validity of the impulse approximation questioned.

Here we present a model for intermediate energy reaction analyses, and for inelastic scattering in particular, that makes use of the nature of distortion in optical model wavefunctions (McCarthy and Pursey 1961; Amos 1967; Janus and McCarthy 1974; Bruce 1981). At intermediate energies the usual distorted wavefunctions may be approximated, at least in the surface region of a nucleus, by attenuated plane waves. These approximations have attendant analytical advantages when used in the derivation of reaction amplitudes and thus yield the analytic distorted wave approximation (ADWA). This approach allows the use of complex, energy and density dependent, two-nucleon t matrices having central, tensor and spin–orbit

0004-9506/83/020135$02.00

characteristics in the analyses of transition data, without necessitating the use of the impulse approximation and its concomitant on-shell limitation, but at the same time making the calculations as simple as those made under the impulse approximation.

The theory of the ADWA for intermediate energy inelastic proton scattering from nuclei is developed in the next section and then later applied to analyse selected reaction data from ^{12}C taken at 402 MeV (Haji-Saeid *et al.* 1982) and at 800 MeV (Blanpied *et al.* 1978). The method is used with the 400 MeV 1^+ transition data to compare three model t matrices, denoted by LF (Love and Franey 1981), PW (Picklesimer and Walker 1978) and Paris (Nakano and von Geramb 1981). This comparison confirms the use of this ADWA and selected reaction data to differentiate between alternative t-matrix properties. The LF force is then used to analyse 800 MeV data and the results further demonstrate the capability of this approach to differentiate between alternative properties of nuclear structure models.

Relevant details of the model t matrices are given in Section 3, whilst those of the nuclear structure models and the results of calculations made using the ADWA are presented in Section 4.

2. Theory

With relativistic kinematics, the inelastic proton scattering differential cross section (in mb sr^{-1}) is given by

$$\mathrm{d}\sigma/\mathrm{d}\Omega = (5/\hat{J}_\mathrm{A})(p_\mathrm{f}/p_\mathrm{i})(E_\mathrm{i}E_\mathrm{f}E_\mathrm{A}E_\mathrm{B}/4\pi^2\bar{s})\sum_{\nu_\mathrm{i}\nu_\mathrm{f}\nu_\mathrm{A}\nu_\mathrm{B}}|T_\mathrm{if}|^2, \tag{1}$$

where all quantities are specified in the c.m. system for the scattering of a proton i from a target A, leaving a residual excited nucleus B and a scattered proton f. All quantities are of standard form, with $\hbar = c = 1$, namely

$$\bar{s} = (E_\mathrm{A}^*+E_\mathrm{i}^*)^2 = \text{invariant mass}, \qquad p_\mathrm{i} = \tfrac{1}{2}\{\lambda(\bar{s}, m_\mathrm{i}^2, M_\mathrm{A}^2)/\bar{s}\}^{\frac{1}{2}}, \tag{2a, b}$$

$$E_\mathrm{i} = (\bar{s}+m_\mathrm{i}^2-M_\mathrm{A}^2)/2\bar{s}^{\frac{1}{2}}, \qquad \lambda(x,y,z) = (x-y-z)^2-4yz\,. \tag{2c, d}$$

Other momenta and energies are similarly defined and, with $\hat{a}$ denoting $2a+1$, the remaining part of equation (1) is the sum (over asymptotic spin projection values) of transition probabilities.

We will assume that the transition amplitudes have the form

$$T_\mathrm{if} = N\langle\chi_\mathrm{f}^{(-)}(0)\psi_\mathrm{B}(1\ldots N)\,|\,t(01)\,|\,\chi_\mathrm{i}^{(+)}(0)\psi_\mathrm{A}(1\ldots N)\rangle, \tag{3}$$

where $t(ab)$ is a two-nucleon t matrix by which the nuclear transition between states J_A and J_B is effected and $\chi^{(\pm)}$ are the relative motion wavefunctions of the projectile.

Standard algebra then enables equation (3) to be recast in a form independent of what model of (microscopic) nuclear structure is chosen as (Amos *et al.* 1978)

$$T_\mathrm{if} = \sum_{j_1j_2I\alpha} S^{(\alpha)}(j_1j_2;J_\mathrm{A}J_\mathrm{B};I)\,\mathscr{M}_{j_1j_2}, \tag{4}$$

where

$$S^{(\alpha)}(j_1j_2;J_\mathrm{A}J_\mathrm{B};I) = S^{(\alpha)}_{j_1j_2} = \langle\psi_{J_\mathrm{B}}\|[a_{j_2}^+\times a_{j_1}]^I_\alpha\|\psi_{J_\mathrm{A}}\rangle \tag{5}$$

are spectroscopic amplitudes (with α denoting a proton or neutron) for the transitions that weight the two-particle matrix elements

$$\mathcal{M}_{j_1 j_2} = \sum_{m_1 m_2 N} (-)^{j_1 - m_1} \langle j_1 j_2 \, m_1 - m_2 \,|\, I - N \rangle \hat{J}_B^{-\frac{1}{2}} \langle J_A I v_A N \,|\, J_B v_B \rangle$$
$$\times \langle \chi_f^{(-)}(0) \, \phi_{j_2 m_2}(1) \,|\, t(01) \,|\, \chi_i^{(+)}(0) \, \phi_{j_1 m_1}(1) \rangle , \tag{6}$$

in which $\phi_{jm}(r)$ are the wavefunctions of the struck bound nucleon, chosen here to be harmonic oscillator wavefunctions ($\hbar\omega$ = 14·9 and 13·9 MeV for ^{12}C and ^{16}O respectively). The projectile relative motion wavefunctions $\chi^{(\pm)}$ are most commonly represented by distorted wave (optical model) functions which then necessitates the use of partial wave expansions in the development of the matrix elements. Simplifying coordinate transformations are thus precluded. For intermediate energies, however, the distortion effects in the spatial region of most relevance for inelastic scattering transition probabilities, namely the nuclear surface, can be well represented by attenuated plane-wave functions (Amos 1967; Janus and McCarthy 1974; Bruce 1981):

$$|\, \chi_i^{(+)}(0) \rangle \approx N_i \exp(i \boldsymbol{K}_i \cdot \boldsymbol{r}_0) \,|\, \tfrac{1}{2} v_i \rangle \,|\, \tfrac{1}{2} \tau_i \rangle , \tag{7a}$$

with

$$\boldsymbol{K}_i = (a + i b) \boldsymbol{k}_i . \tag{7b}$$

The parameters a and b may be estimated from a local WKB approximation and/or by fitting scattering data (Janus and McCarthy 1974) with the normalization factor N_i set to yield unit amplitudes for the continuum functions at the nuclear surface. A better scheme to choose the parameter values is to use the attenuated plane-wave function in the Born approximation integral with the appropriate optical model potential and thereby fit elastic scattering data (Bruce 1981). Whatever the method of fixing parameters, the form of the attenuated plane waves facilitates a transformation of coordinates in the two-particle matrix elements to give

$$\mathcal{M}_{j_1 j_2} = \sum_{m_1 m_2 N} (-)^{j_1 - m_1} \langle j_1 j_2 \, m_1 - m_2 \,|\, I - N \rangle \hat{J}_B^{-\frac{1}{2}} \langle J_A I v_A N \,|\, J_B v_B \rangle N_i N_f$$
$$\times \langle \tfrac{1}{2} v_f \,|\, \langle \tfrac{1}{2} \tau_f \,|\, \langle \exp(i \boldsymbol{K}_f \cdot \boldsymbol{r}) \,|\, t(r) \,|\, \exp(i \boldsymbol{K}_i \cdot \boldsymbol{r}) \rangle$$
$$\times \langle \exp(i \boldsymbol{K}_f \cdot \boldsymbol{r}_1) \, \phi_{j_2 m_2}(1) \,|\, \exp(i \boldsymbol{K}_i \cdot \boldsymbol{r}_1) \, \phi_{j_1 m_1}(1) \rangle \,|\, \tfrac{1}{2} v_i \rangle \,|\, \tfrac{1}{2} \tau_i \rangle . \tag{8}$$

Thus the t matrix and nuclear structure aspects of intermediate energy reaction amplitudes separate (as with the impulse approximation), and standard angular momentum algebra with a t matrix of the form (where c, t and s.o. denote central, tensor and spin–orbit potentials respectively)

$$t(01) = \sum_{ST} v_{ST}^{c}(01) \, P^S P^T + \sum_{T} v_T^{t}(01) \, S_{01} \, P^T + \sum_{T} v_T^{s.o.}(01) \, (\boldsymbol{L} \cdot \boldsymbol{S}/\hbar^2) P^T \tag{9}$$

yields 'analytic' matrix elements. Hence we get the ADWA of

$$T_{if}^{c} = \sum N_i N_f S_{j_1 j_2}^{(\alpha)} 2\pi i^L (-)^{S+L+1+j_1-j_2} \hat{L} \hat{S} \hat{\Gamma} (2 \hat{l}_1 \hat{j}_1 \hat{j}_2 / \hat{J}_B)^{\frac{1}{2}} \langle v_{ST}^{c}(Q) \rangle_0$$
$$\times \langle J_A I v_A N \,|\, J_B v_B \rangle \langle \tfrac{1}{2} \Gamma v_f N \,|\, \tfrac{1}{2} v_i \rangle \begin{pmatrix} \frac{1}{2} & \frac{1}{2} & \Gamma \\ \frac{1}{2} & \frac{1}{2} & S \end{pmatrix} \langle R_{l_2 j_2} R_{l_1 j_1}(Q) \rangle_L \langle \tfrac{1}{2} \tfrac{1}{2} \tau_i \alpha \,|\, T M_T \rangle \times$$

$$\times \langle \tfrac{1}{2}\tfrac{1}{2}\tau_f \alpha \,|\, TM_T\rangle \langle l_1 L00 \,|\, l_2 0\rangle \langle L\Gamma 0 - N \,|\, I - N\rangle \begin{pmatrix} \frac{1}{2} & \frac{1}{2} & \Gamma \\ l_2 & l_1 & L \\ j_2 & j_1 & I \end{pmatrix}, \tag{10a}$$

$$T^{t}_{if} = \sum N_i N_f S^{(\alpha)}_{j_1 j_2} 8\pi i^L \langle J_A I v_A N \,|\, J_B v_B\rangle \hat{L}\hat{\Gamma}\hat{F}(3\hat{I}_1\hat{j}_1\hat{j}_2/\hat{J}_B)^{\frac{1}{2}}$$
$$\times \langle \tfrac{1}{2}\tfrac{1}{2}\tau_i \alpha \,|\, TM_T\rangle \langle \tfrac{1}{2}\tfrac{1}{2}\tau_f \alpha \,|\, TM_T\rangle \langle l_1 L00 \,|\, l_2 0\rangle \langle L\Gamma 0N \,|\, IN\rangle \langle \tfrac{1}{2} F v_i \delta \,|\, \tfrac{1}{2} v_f\rangle$$
$$\times \langle \Gamma F N\delta \,|\, 20\rangle \begin{pmatrix} \Gamma & L & I \\ \frac{1}{2} & l_1 & j_1 \\ \frac{1}{2} & l_2 & j_2 \end{pmatrix} \begin{pmatrix} F & \Gamma & 2 \\ \frac{1}{2} & \frac{1}{2} & 1 \\ \frac{1}{2} & \frac{1}{2} & 1 \end{pmatrix} \langle v^t_T(Q)\rangle_2 \langle R_{l_1 j_1} R_{l_2 j_2}(Q)\rangle_L, \tag{10b}$$

$$T^{s,o\cdot}_{if} = \sum N_i N_f S^{(\alpha)}_{j_1 j_2} 6\pi i^L \langle J_A I v_A N \,|\, J_B v_B\rangle \hat{L}\hat{\Gamma}\hat{F}(2\hat{I}_1\hat{j}_1\hat{j}_2/\hat{J}_B)^{\frac{1}{2}} \langle l_1 L00 \,|\, l_2 0\rangle$$
$$\times \langle \tfrac{1}{2}\tfrac{1}{2}\tau_i \alpha \,|\, TM_T\rangle \langle \tfrac{1}{2}\tfrac{1}{2}\tau_f \alpha \,|\, TM_T\rangle \langle \tfrac{1}{2} F v_i \delta \,|\, \tfrac{1}{2} v_f\rangle \langle L\Gamma 0N \,|\, IN\rangle \langle \Gamma F N\delta \,|\, 1\xi\rangle \,|\, \xi \,|$$
$$\times \begin{pmatrix} F & \Gamma & 1 \\ \frac{1}{2} & \frac{1}{2} & 1 \\ \frac{1}{2} & \frac{1}{2} & 1 \end{pmatrix} \begin{pmatrix} \Gamma & L & I \\ \frac{1}{2} & l_1 & j_1 \\ \frac{1}{2} & l_2 & j_2 \end{pmatrix} (K_i^2 - \tfrac{1}{4}Q^2)^{\frac{1}{2}} \langle r\, v^{s,o\cdot}_T(Q)\rangle_1 \langle R_{l_1 j_1} R_{l_2 j_2}(Q)\rangle_L. \tag{10c}$$

The summations extend over the quantum numbers $L, T, I, j_1, j_2, \Gamma, F$ and α. The radial expectation values are

$$\langle G(Q)\rangle_k = \int \mathrm{j}_k(Qr)\, G(r)\, r^2\, \mathrm{d}r, \tag{11}$$

involving the complex momentum transfer

$$\boldsymbol{Q} = \boldsymbol{K}_i - \boldsymbol{K}_f, \tag{12}$$

which for intermediate energies (and thus negligible q values insofar as parameter variation is concerned) gives the 'magnitude'

$$Q = (a + \mathrm{i}\, b)(2m_i^2 - 2E_i E_f + 2p_i p_f \cos\theta_{sc})^{\frac{1}{2}} \tag{13}$$

appearing in the argument of the spherical Bessel functions j_k of equation (11). The structure radial expectation values in equations (10) involve functions $R_{lj}(r)$ which are the bound state (harmonic oscillator) radial wavefunctions. The relevant steps in the derivation of the matrix elements of equations (10) are given in the Appendix.

Thus the ADWA for inelastic scattering gives matrix elements that yield readily to computation and in which momentum transfer properties of the two-nucleon t matrix and momentum transfer properties of nuclear spectroscopy are effectively separated. Given then the validity of the ADWA, we have a convenient scheme to study one or the other of those momentum transfer properties.

Naturally, a collective model prescription of intermediate energy scattering can also be entertained. With the ADWA it is a simple exercise to deduce that for the excitation of states ψ_{J_B} from zero spin ground states

$$\mathrm{d}\sigma/\mathrm{d}\Omega \propto (\beta_{J_B} R_0)^2 \,|\, \langle \partial U/\partial r(Q)\rangle_{J_B} \,|^2, \tag{14}$$

where $U(r)$ is the usual optical model potential with R_0 the nuclear radius and β_{J_B} the deformation parameter.

3. Model t Matrices

In the calculations three model t matrices have been used, and their momentum transfer properties, together with data from inelastic scattering on nuclei, are displayed in Figs 1–6. In all cases the Love–Franey (1981) (LF) model t matrix properties are displayed by the solid curves. Properties of the Picklesimer–Walker (1978) (PW) model t matrix are displayed by the long-dashed curves, whilst those of a model t matrix based upon the Paris two-nucleon interaction are shown by the short-dashed curves. All model t matrices are complex and by using the form

$$t(r) = t_R(r) - i\, t_I(r), \tag{15}$$

with real values for q, we get the momentum functions $4\pi\langle r^L t_R(q)\rangle_L$ and $4\pi\langle r^L t_I(q)\rangle_L$ presented in Figs 1–6, with $L = 0$, 1 and 2 for the central, spin–orbit and tensor components respectively. The functions $\langle t(q)\rangle_L$ can change sign so that negative values are indicated in the figures by dots.

All three model t matrices are combinations of Yukawa functions, i.e.

$$V^{\text{type}}_{(S)T}(r) = \sum_i W^{\text{type}}_{(S)T}(i) \exp(-\mu_i r)/\mu_i r, \tag{16}$$

with complex weights $W(i)$. In the LF model t matrix, these weights are also (projectile) energy dependent, as are those of the Paris model t matrix. The Paris model t matrix has momentum dependences as well, as a result of density dependent strengths. We display the momentum properties of the single set corresponding to a local Fermi momentum of $1{\cdot}0\ \text{fm}^{-1}$. From the local density equivalence and a density

$$\rho(r) = 0{\cdot}156/[1{\cdot}0 + \exp\{(r - 2{\cdot}747)/0{\cdot}57\}],$$

this is the local infinite matter t matrix at a radius of $2{\cdot}9$ fm.

The PW model t matrix was derived by Picklesimer and Walker (1978) by fitting nucleon–nucleon scattering data (differential cross sections and polarizations) between 50 and 400 MeV. With complex but energy independent coefficients, quite reasonable fits to data were reported, although the sensitivity of the predictions to parameter variations was not. Further, the use by Picklesimer and Walker of the PW t matrix in analyses of inelastic scattering data was inconclusive as a test of the t-matrix model because of the oversimplified nuclear structure and the plane-wave approximation (at 156 MeV) employed.

The LF model t matrix of Love and Franey (1981) was generated in a similar manner to the PW version, albeit the complex coefficients of the set of Yukawa interactions were allowed to be energy dependent and were determined using a χ^2 search procedure to fit the two-nucleon scattering amplitude deduced from phase shift analyses of data. The uncertainties in the t matrix were also discussed and a number of applications in inelastic proton scattering and charge exchange reaction analyses were made. But as with the PW study, the nuclear structure input was simplistic.

The third model t matrix to be used was developed from the free nucleon–nucleon Paris potential (Lacombe *et al.* 1980) by Nakano and von Geramb (1981) to obtain a local energy and density dependent t matrix from the Bethe–Goldstone equation. The result was then mapped onto a combination of Yukawa functions for each local Fermi momentum of a Woods–Saxon matter distribution.

Parameter values for the three model t matrices are not given here, as both the PW and LF sets of parameters are available in the literature, whilst those of the Paris model are very extensive and may be obtained from the University of Hamburg.

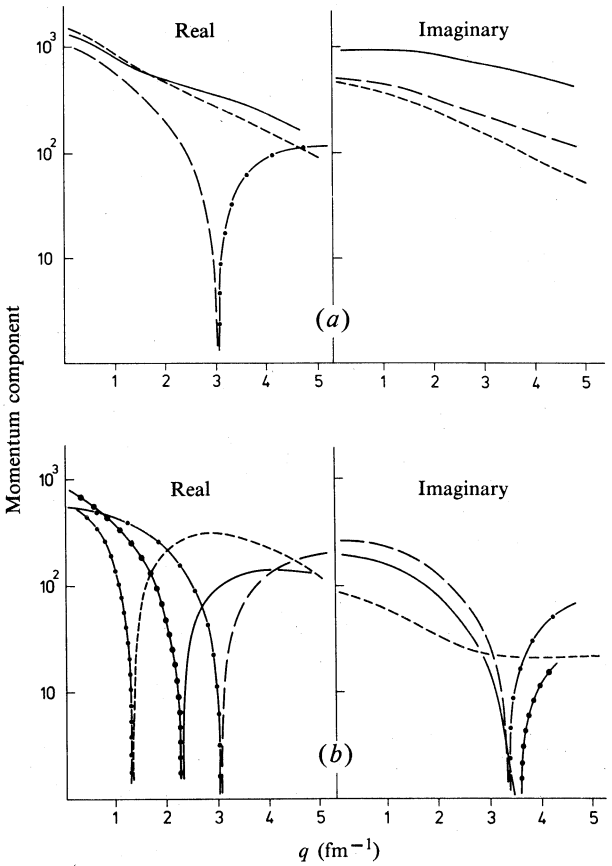

Fig. 1. Momentum components of (*a*) the singlet-odd and (*b*) the singlet-even central force t matrices at 400 MeV incident proton energy: solid curves, the LF model t matrix; long-dashed curves, the PW model t matrix; short-dashed curves, the Paris model t matrix. The dots indicate negative values.

The three model t matrix momentum components for a projectile energy of 400 MeV are compared in Figs 1–4. The LF t matrix is in fact that quoted for 425 MeV.

The singlet-odd state t-matrix momentum components are displayed in Fig. 1*a*. This two-body spin channel ($S = 0$) has only central force contributions with the LF and Paris forces (solid and short-dashed curves respectively) having similar short-range repulsive character; the LF t matrix has a stronger imaginary component. The PW t matrix in this channel (long-dashed curve) has an imaginary part quite like that of the Paris model, but its real component has a short-range attractive part that causes very small momentum (real part) components near 3 fm^{-1}. However, as angular momentum and isospin selection minimize the effect of this channel in transitions, it is unlikely that nuclear reaction data will test such differences. Certainly,

the transitions considered here with spin and/or isospin flip character will not be influenced to any extent by this channel.

The singlet-even and triplet-even channels (the Serber force part) play more significant roles in transition data analyses and the central force components of these t matrices are shown in Figs 1*b* and 2*a*. The real components are all of long-range attractive plus short-range repulsive character, with the Paris model t matrix having a further very short-range attraction. The singlet-even (real) forces reach a counterbalance of attraction and repulsion at approximately 0·3, 0·5 and 0·7 fm for the PW, LF and Paris model t matrices respectively. The LF and PW singlet-even imaginary components in Fig. 1*b* are very similar with again a long-range attraction plus short-range repulsion being the net effect of the Yukawa combinations, whereas that of the Paris model is again a three region quantity with a very weak repulsive region between 0·4 and 0·6 fm.

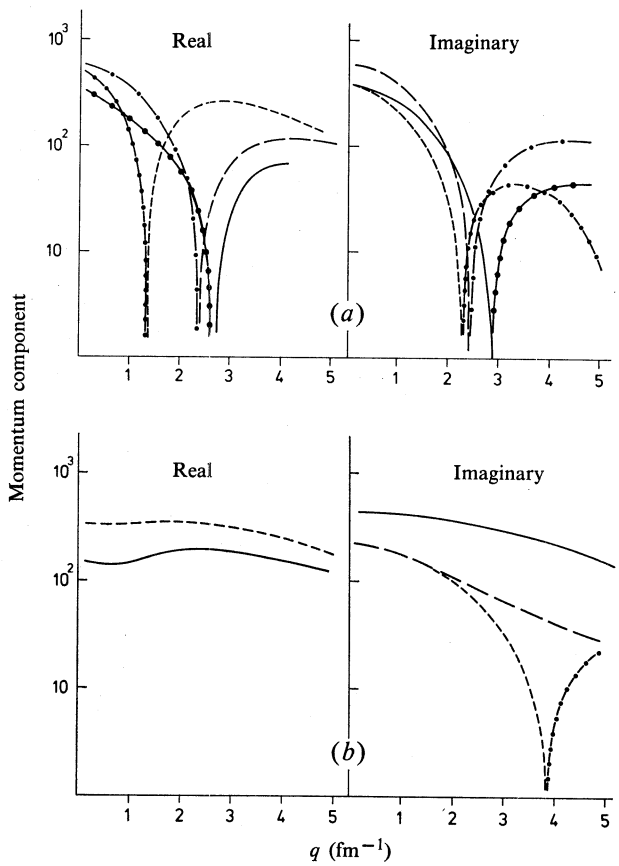

Fig. 2. Momentum components of (*a*) the triplet-even and (*b*) the triplet-odd central force t matrices at 400 MeV incident proton energy (see caption to Fig. 1). In (*b*) there is no real part in the PW interaction.

The triplet-even central forces in Fig. 2*a* are also basically long-range attraction with short-range repulsion, with counterbalance radii of 0·4 fm for both the LF and PW real and imaginary components. The Paris t matrix in this channel has an additional very short-range attraction, whence counterbalance radii of 0·2 and 0·8 fm and

0·3 and 0·6 fm result for the real and imaginary parts respectively. The net effect so far as momentum components are concerned is that the imaginary parts of all t matrices are relatively similar compared with the distinct difference between the real parts of the Paris and LF or PW forces.

The triplet-odd channel central force components are shown in Fig. 2*b*. All forces have distinctive momentum components with the LF and Paris real components having a very short-range repulsive character; there is no real component PW force in this channel. The imaginary components of the LF and PW forces are similar, having short-range attraction in this channel. The Paris force on the other hand has a short-range repulsion with long-range attraction and a balance radius of about 1 fm. In fact, the real components do have a long-range, but relatively weak, attractive character.

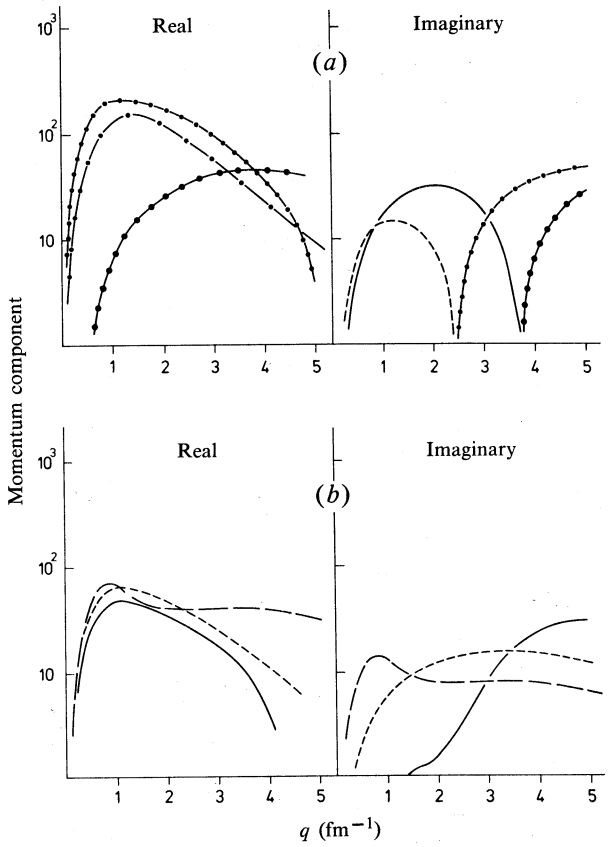

Fig. 3. Momentum components of (*a*) the triplet-even and (*b*) the triplet-odd tensor force t matrices at 400 MeV incident proton energy (see caption to Fig. 1). In (*a*) there is no imaginary part in the PW interaction.

The momentum components of the tensor forces are displayed in Figs 3*a* and 3*b* for the triplet-even and triplet-odd terms respectively. The individual t matrices have quite distinctive characteristics in both channels with the PW triplet-even channel force being purely real. In the triplet-even channel the LF force real component is purely attractive, whereas the PW and Paris forces have additionally a short-range

repulsion with a balance at 0·2 and 0·6 fm respectively. The imaginary components of both the LF and Paris forces have a long-range attraction with a short-range repulsion to counterbalance at 0·8 and 1·0 fm respectively. The momentum components of the tensor force t matrices in the triplet-odd channel of Fig. 3*b* are similarly disparate with all real components being repulsive, with short-range attractions in both the LF (0·7 fm) and Paris (0·4 fm) cases. The PW and Paris forces have purely attractive imaginary components, whilst the LF imaginary term has a weak repulsive region between 1·0 and 2·0 fm.

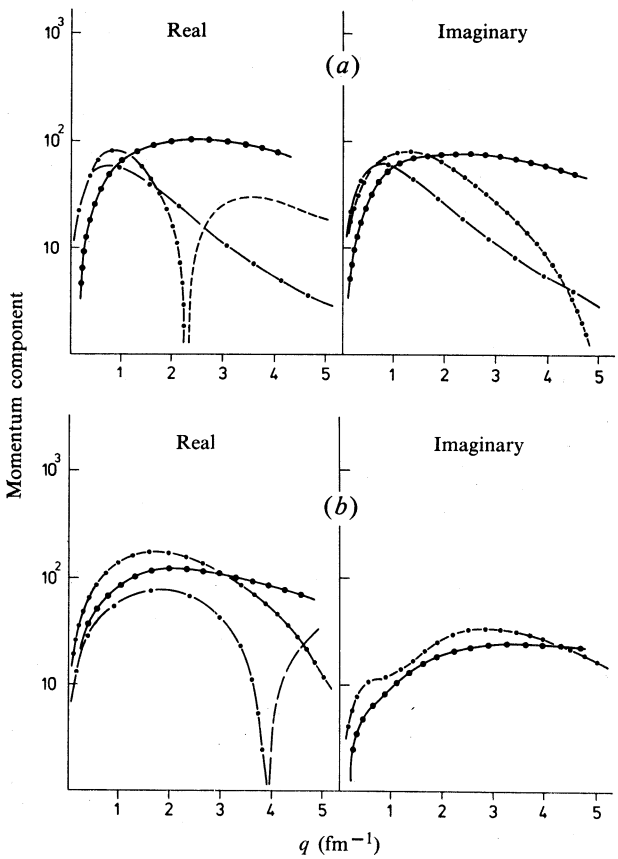

Fig. 4. Momentum components of (*a*) the triplet-even and (*b*) the triplet-odd spin–orbit force t matrices at 400 MeV incident proton energy (see caption to Fig. 1). In (*b*) there is no imaginary part in the PW interaction.

The momentum components of the spin–orbit forces of the three t matrices are as dissimilar as those of the tensor forces. They are displayed for the triplet-even and triplet-odd channels in Figs 4*a* and 4*b* respectively. In the former the PW and LF forces are purely attractive (real) and purely repulsive (imaginary). The Paris force on the other hand has also a short-range repulsive region, between 0·3 and 1 fm for the real component and for all radii less than 0·3 fm for its imaginary component. In the triplet-odd channel (Fig. 4*b*) the spin–orbit t matrices have basically a long-range attraction for the real part and a fairly short-range repulsive character for the

imaginary part, save for the non-existent PW imaginary term. Both the PW and Paris model t matrices have a short-range repulsive term in their real components with counterbalance radii of 0·6 and 0·4 fm respectively.

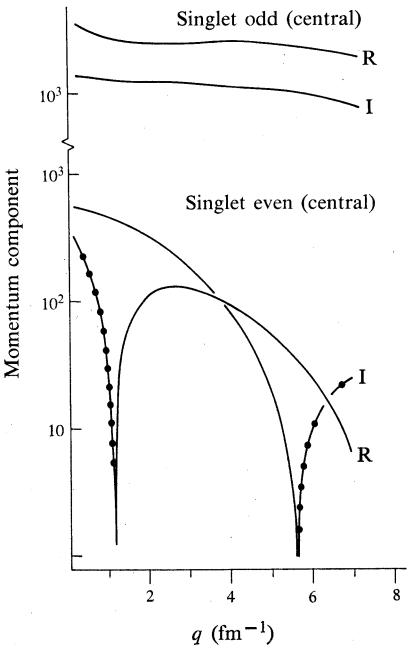

Fig. 5. Real (R) and imaginary (I) momentum components of the singlet (central) forces in the LF matrix at 800 MeV incident energy. Dots indicate negative values.

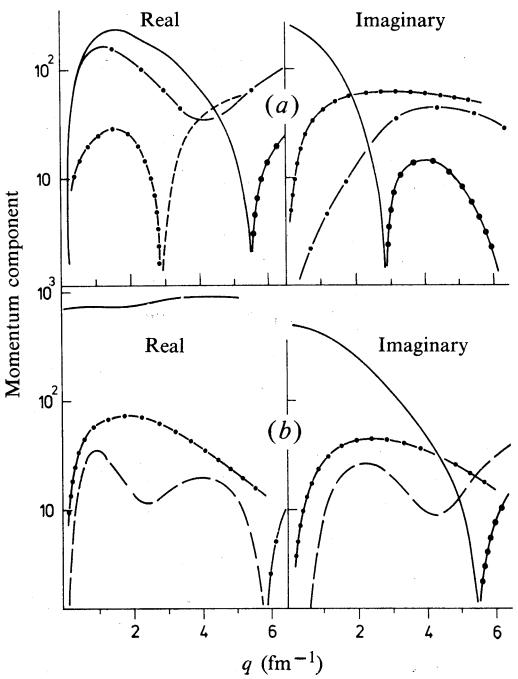

Fig. 6. Momentum components of (*a*) the triplet-even and (*b*) the triplet-odd forces in the LF t matrix at 800 MeV incident energy. The central, tensor and spin–orbit components are shown by the solid, long-dashed and short-dashed curves respectively.

Of the three t matrices, only the LF model has been parametrized to match 800 MeV data and the associated momentum components are given in Figs 5 and 6. In Fig. 5, the singlet channel (purely central) values are displayed, with R and I denoting the real and imaginary parts. The momentum components of the central, tensor and spin–orbit components of the 800 MeV LF model t matrix are shown in Fig. 6 by the solid, long-dashed and short-dashed curves respectively. These momentum distributions are clearly associated with a complicated coordinate space variation of forces. A simplified graphic representation of the coordinate space variation is given in Fig. 7; lower case characters denote weak repulsion and attraction regions.

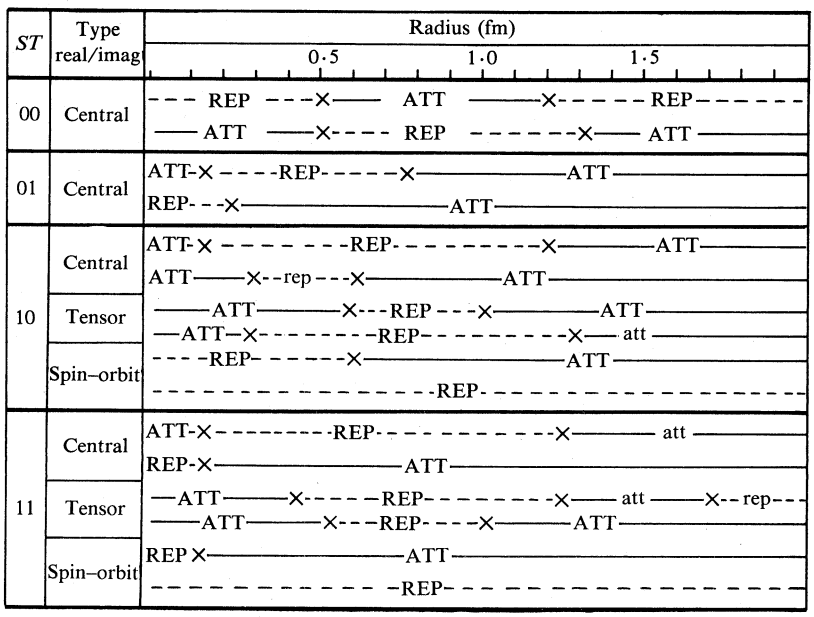

Fig. 7. Schematic of the coordinate space variations of the components of the 800 MeV LF t matrix.

4. Inelastic Scattering Results

The ADWA method has been used with the t matrices described in the previous section to analyse selected 402 MeV and 800 MeV incident energy inelastic proton scattering data from ^{12}C. Specifically, the transition data from the excitation of the isoscalar and isovector 1^+ (at 12·71 and 15·11 MeV) and 2^+ (at 4·44 and 16·11 MeV) states have been considered. A shell model (SM), a large basis particle–hole model (PHM) and a projected Hartree–Fock Born approximation model (PHFBAM) of nuclear structure have been used in these studies to ascertain the spectroscopic amplitudes $S^{(\alpha)}_{j_1 j_2}$ required in the analyses. The proton values $S^{(-\frac{1}{2})}_{j_1 j_2}$ are listed in Table 1 for the 1^+ state transitions and in Table 2 for the 2^+ state transitions. For these cases the neutron amplitudes have the same values modulated by a phase of $(-1)^{J+T}$ for each transition (to a state $|\psi_{JT}\rangle$). Clearly the 1^+ state excitations are dominated by transitions within the 0p shell and, indeed, spectral properties favour the SM prescription to that of the PHM (Amos *et al.* 1981). Strong 0p shell transitions should also be evident in the 2^+ state excitations as can be seen from the spectroscopic amplitudes of Table 2. But important contributions from other shells can be expected

Table 1. Proton spectroscopic amplitudes for excitation of isoscalar (12·71 MeV) and isovector (15·11 MeV) 1^+ states in ^{12}C

		$S(j_1 j_2; 01; 1)$			
		$T = 0$		$T = 1$	
j_1	j_2	SM	PHM	SM	PHM
0p1	0p1	0·053	0·066	−0·071	0·128
0p3	0p1	−0·880	−0·644	−0·845	−0·578
1p1	0p1		0·007		−0·014
1p3	0p1		−0·092		−0·084
0p1	0p3	−0·434	−0·461	−0·416	−0·490
0p3	0p3	−0·017	−0·027	−0·093	−0·167
1p1	0p3		−0·052		−0·055
1p3	0p3		−0·011		−0·032
0f5	0p3		0·003		0·011
0s1	1s1		0·023		0·016
0s1	0d3		0·136		−0·047
1s1	0d3		0·019		−0·006
0p1	1p1		0·060		−0·020
0p3	1p1		−0·010		−0·005
0p1	1p3		−0·026		0·025
0p3	1p3		0·008		0·031
0p3	0f5		0·081		−0·027
1p3	0f5		0·010		−0·004
0f7	0f5		−0·004		−0·011

Table 2. Proton spectroscopic amplitudes for 2^+ state excitations in ^{12}C

Three model results for the isoscalar (4·44 MeV) state excitation are compared with those for the isovector (16·11 MeV) state excitation

		$S(j_1 j_2; 02; 2)$			
j_1	j_2	SM ($T = 0$)	PHFBAM ($T = 0$)	PHM ($T = 0$)	PHM ($T = 1$)
0d3	0s1		−0·114	−0·170	
0d5	0s1		−0·128	−0·184	
0p3	0p1	−1·195	−1·086	−0·935	−0·393
1p3	0p1		−0·054	−0·141	−0·049
0f5	0p1		−0·045	−0·025	−0·016
0p1	0p3	0·704	0·804	0·845	0·354
0p3	0p3	0·503	0·549	0·654	−0·725
1p1	0p3			0·095	−0·040
1p3	0p3			0·069	−0·093
0f5	0p3			−0·074	−0·012
0f7	0p3		−0·064	−0·121	
0d3	1s1			−0·025	
0s1	0d3		0·209	0·203	
1s1	0d3			0·028	
0s1	0d5		−0·234	−0·211	0·012
1s1	0d5			−0·029	
0p3	1p1			−0·097	
0p1	1p3			0·131	−0·014
0p3	1p3		0·043	0·055	0·033
0p1	0f5		−0·056	−0·101	−0·028
0p3	0f5		0·088	0·108	−0·039
0p3	0f7		−0·197	−0·225	−0·015

and they do in fact occur (Amos and Morrison 1979; Amos *et al.* 1981). In particular the PHFBAM spectroscopy not only predicts the B(E2) value, the longitudinal electron scattering form factor (to $q \sim 2$ fm^{-1} at least) and the lower energy (60 MeV) inelastic proton scattering cross sections in good agreement with data, but also, to within a scaling, the transverse electron scattering form factor. As such, the PHFBAM may be considered the 'correct' spectroscopy against which the other model predictions can be compared, and it will be seen that high energy (800 MeV) pp′ data are not only consistent with the correct spectroscopy, but also select between analyses with different model spectroscopies in the same fashion as the low energy data analyses.

In Fig. 8 the ADWA analyses of the 1^+ transitions initiated by 402 MeV protons are compared with the data of Haji-Saeid *et al.* (1982). Attenuation parameters a, b and N of 1·05, 0·04 and 0·61 were used to obtain the isovector transition predictions. These were varied to 1·2, 0·015 and 0·83 for the isoscalar transitions simply to improve the fit from poor to the less than satisfactory results displayed. In common with previous analyses of lower energy data (Love and Franey 1981; Amos *et al.* 1981), the isoscalar 1^+ excitation in ^{12}C remains a mystery. In the calculations (the results of which are depicted by the solid curve for the LF t matrix, the dot–dash curve for the PW t matrix and the dashed curve for the Paris t matrix) the SM nuclear structure was used. The set labelled C + T in the 12·71 MeV state analysis was obtained by omitting the spin–orbit components of each t matrix. The variation in structure and magnitude of predictions caused by the spin–orbit force is most evident. Thus, in part at least, the mystery of the isoscalar 1^+ transition rests with the proper spin–orbit attribute of the two-nucleon t matrix. The tensor and, to a lesser extent, the central force components of the t matrices dominate analyses of the isovector transition, and as with lower energy data analyses, the data are fit quite well. In both cases the LF t matrix calculations give the best comparison with experiment.

At 800 MeV, only the LF t matrix has been defined to date and hence in Figs 9–11 in which 800 MeV data are compared with ADWA predictions all such predictions, save for collective model calculations, were obtained using this matrix. In Fig. 9, the ^{12}C isoscalar and isovector 1^+ excitation data are compared with ADWA predictions made using the SM (solid curve) and PHM (dashed curve) spectroscopic amplitudes given in Table 1. The ADWA parameter values of 1·05, 0·035 and 0·54 for a, b and N respectively used to obtain the isovector fits were varied again to try and improve the comparison with the isoscalar transition data. Values of 1·0, 0·06 and 0·35 give the 12·71 MeV results. The isovector data are fitted quite well using the SM structure and the isoscalar results are quite reasonable. The PHM structure results, however, are quite distinct and give poor predictions. Thus, these data do differentiate between nuclear structure models. Furthermore, at this projectile energy a variation in structure between that of the 0p shell SM and the large basis PHM may result in a good fit to data. This suggests the use of the 800 MeV data to fix a credible model structure for the isoscalar 1^+ transition, which may then be used in lower energy data analyses to seek improvements to the t matrices.

To complement analyses of the 1^+ unnatural parity transitions in ^{12}C as a test of the t matrix, we analysed as well the data from 800 MeV inelastic proton scattering to the 2^-(8·88 MeV) isoscalar state in ^{16}O and to the 2^+(16·11 MeV) isovector state in ^{12}C. Again the ADWA parameters were adjusted to optimize a fit to data with respective values of (1·0, 0·074, 0·24) and (1·15, 0·046, 0·45) for (a, b, N) being used

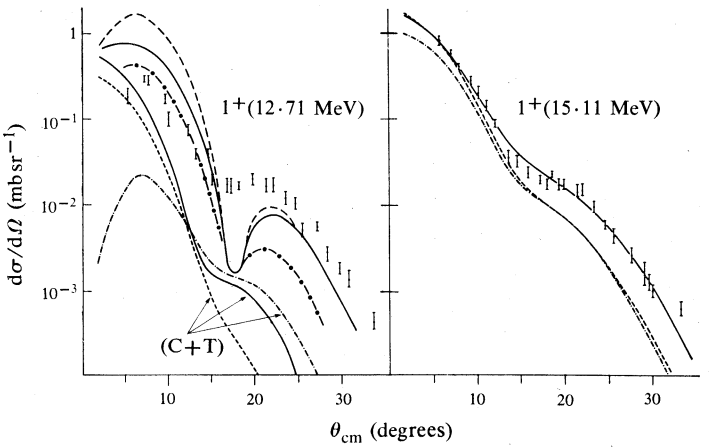

Fig. 8. Comparison of the ADWA predictions using the various two-nucleon t matrices with data (Haji-Saeid *et al.* 1982) from the inelastic scattering of 402 MeV protons exciting the isoscalar $1^+(12{\cdot}71$ MeV) and isovector $1^+(15{\cdot}11$ MeV) states in ^{12}C. The curves are identified in the text and all were obtained using SM spectroscopy.

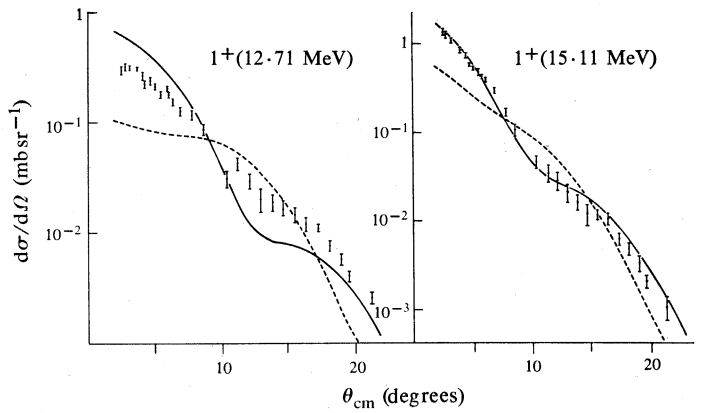

Fig. 9. ADWA predictions obtained using the LF two-nucleon t matrix and compared with the inelastic scattering data (Blanpied *et al.* 1978) from 800 MeV proton excitation of the isoscalar $1^+(12{\cdot}71$ MeV) and isovector $1^+(15{\cdot}11$ MeV) states in ^{12}C. The solid curve depicts the results when SM spectroscopy was used, whilst the dashed curve gives those from PHM spectroscopy.

to get the ^{16}O and ^{12}C predictions displayed in Fig. 10. Use of a standard collective model form factor for the isovector 2^+ state transition gave the results depicted by the dashed curve. The good fit suggests that the ADWA method is reasonable for analysis of any spin and/or isospin flip transition. That this is also the case for non-spin and isospin flip transitions as well is shown by the good fit to data, at least for low momentum transfer values, of our ADWA calculations made using the 'correct' PHFBAM spectroscopy for the excitation of the $2^+(4{\cdot}44$ MeV) state in ^{12}C. The results are displayed in Fig. 11 where the PHFBAM spectroscopy results are shown by the solid curve, whilst those obtained using the PHM and SM spectroscopic

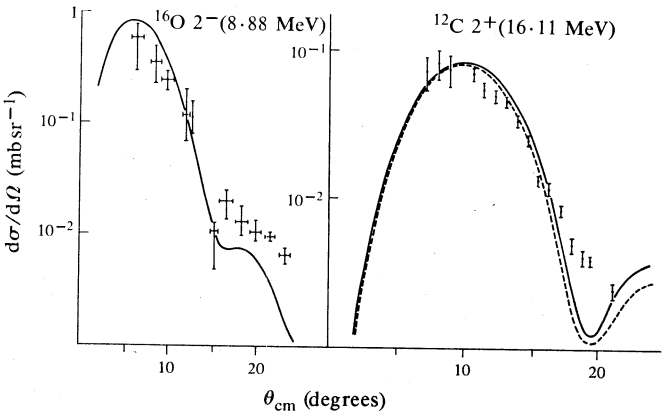

Fig. 10. Comparison with 800 MeV data (Blanpied *et al.* 1978) of ADWA calculations for excitation of the 2^- state in ^{16}O and the isovector 2^+ state in ^{12}C, using the LF interaction. The ^{16}O spectroscopic amplitudes were obtained from a SM calculation, whilst those for ^{12}C were obtained from the PHM. The dashed curve is the result of an (unnormalized) collective model calculation.

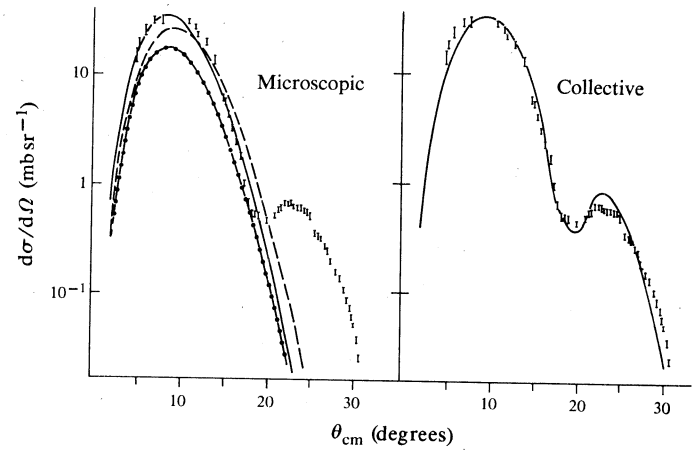

Fig. 11. Comparison of ADWA calculations with data (Blanpied *et al.* 1978) from the excitation of the 2_1^+ state in ^{12}C initiated by 800 MeV protons. The microscopic model calculations used the LF two-nucleon t matrix with SM (dot–dash curve), PHM (dashed curve) and PHFBAM (solid curve) spectroscopic amplitudes.

amplitudes are depicted by the dashed and dot–dash curves respectively. The better fit of the PHFBAM values compared with those of the PHM (in shape) and the SM (in magnitude and shape) is quite evident, and this was also noted in another study of this reaction but at a lower projectile energy (Amos and Morrison 1979). It is intriguing to observe that the second peak in the measured data can be reproduced by the usual collective model prescription. To do so, however, requires that we use an optical potential of V_0(20·0 MeV), r_0(1·2 fm), a_0(0·55 fm), W_0(38·0 MeV), r_d(1·35 fm) and a_d(0·45 fm), with a deformation parameter β_2 of 0·625 and ADWA parameters of (0·85, 0·021, 0·69) for (a, b, N). Though the microscopic form factors

involve a folding of the two-nucleon t matrix, this result suggests that the nuclear structure properties of the transition, other than those of the dominant p–s–d shells, may be the significant factor in the high momentum transfer region of this data.

5. Conclusions

An analytic distorted wave approximation has been specified for use in analyses of medium energy inelastic proton scattering data. With a simple form for the continuum (proton) wavefunctions, transition amplitudes involving central, tensor and two-body spin–orbit force components in the two-nucleon t matrix have been specified which are amenable for predicting differential cross sections even with very large basis nuclear structure information.

Use of this model prescription in analyses of a selected set of transition data, namely the excitation of the 1^+ isoscalar and isovector states in ^{12}C at 402 and 800 MeV and of the 2^+ isoscalar and isovector states in ^{12}C at 800 MeV, demonstrates not only that a clear definition between complex models of the two-nucleon t matrices and between models of nuclear structure exists in the predictions, but also that data are fitted by the most appropriate predictions. Though details of the model need refining, for example, the removal of the arbitrary way in which the attenuation parameter values are selected, the ADWA has nevertheless been established as a viable method of data analysis, one which is competitive with the DWIA. Furthermore, by retaining off-shell dependences in the t matrices, the ADWA is a distinct improvement over the usual form of the DWIA.

Acknowledgment

One of us (F.Di M.) acknowledges the financial support of a Commonwealth Postgraduate Research Award.

References

Amos, K. (1967). *Nucl. Phys.* **77**, 225.
Amos, K., Faessler, A., Morrison, I., Smith, R., and Muether, H. (1978). *Nucl. Phys.* A **304**, 191.
Amos, K., and Morrison, I. (1979). *Phys. Rev.* C **19**, 2108.
Amos, K., Morrison, I., Smith, R., and Schmid, K. (1981). *Aust. J. Phys.* **34**, 493.
Blanpied, G. S., *et al.* (1978). *Phys. Rev.* C **18**, 1436.
Bruce, I. (1981). Thesis, Flinders University of South Australia, Rep. No. FIAS-R-78.
Haji-Saeid, M., *et al.* (1982). *Phys. Rev.* C **25**, 3035.
Janus, R. T., and McCarthy, I. E. (1974). *Phys. Rev.* C **10**, 1041.
Lacombe, M., Loisau, B., Richard, J. M., Vinh Mau, R., Côté, J., Pirès, P., and de Tourreil, R. (1980). *Phys. Rev.* C **21**, 861.
Love, W. G., and Franey, M. A. (1981). *Phys. Rev.* C **24**, 1073.
McCarthy, I. E., and Pursey, D. (1961). *Phys. Rev.* **122**, 578.
Nakano, K., and von Geramb, H. V. (1981). Tables of effective density and energy dependent interactions for nucleons. Hamburg University Report.
Picklesimer, A., and Walker, G. E. (1978). *Phys. Rev.* C **17**, 237.

Appendix. Derivation of Matrix Elements

Central Forces

Using the central force component of a t matrix (see equation 9) in the matrix elements (8) and expanding the bound state wavefunctions gives

$$\mathcal{M}^{c}_{j_1 j_2} = \sum (-)^{j_1 - m_1} \langle j_1 j_2 m_1 - m_2 \,|\, I - N \rangle \hat{J}_B^{-\frac{1}{2}} \langle J_A I \nu_A N \,|\, J_B \nu_B \rangle N_i N_f \langle \tfrac{1}{2}\tfrac{1}{2} \nu_i \mu_1 \,|\, S M_S \rangle$$
$$\times \langle \tfrac{1}{2}\tfrac{1}{2} \nu_f \mu_2 \,|\, S M_S \rangle \langle \tfrac{1}{2}\tfrac{1}{2} \tau_i \alpha \,|\, T M_T \rangle \langle \tfrac{1}{2}\tfrac{1}{2} \tau_f \alpha \,|\, T M_T \rangle$$
$$\times \langle l_1 \tfrac{1}{2} m_{l_1} \mu_1 \,|\, j_1 m_1 \rangle \langle l_2 \tfrac{1}{2} m_{l_2} \mu_2 \,|\, j_2 m_2 \rangle$$
$$\times \int d\boldsymbol{r}_0 \int d\boldsymbol{r}_1 \exp\{ i (\boldsymbol{K}_i - \boldsymbol{K}_f) . \boldsymbol{r}_0 \} V^{c}_{ST}(r_{01})$$
$$\times R_{l_1 j_1}(r_1) R_{l_2 j_2}(r_1) Y^{*}_{l_2 m_{l_2}}(\Omega_1) Y_{l_1 m_{l_1}}(\Omega_1) . \tag{A1}$$

Transforming to variables $\boldsymbol{r}$ $(= \boldsymbol{r}_0 - \boldsymbol{r}_1 = \boldsymbol{r}_{01})$ and $\boldsymbol{r}_1$ and expanding the 'plane' waves in multipoles, with $\boldsymbol{Q} = \boldsymbol{K}_i - \boldsymbol{K}_f$, then yields

$$\mathcal{M}^{c}_{j_1 j_2} = \sum \hat{J}_B^{-\frac{1}{2}} \langle J_A I \nu_A N \,|\, J_B \nu_B \rangle \langle \tfrac{1}{2}\tfrac{1}{2} \tau_i \alpha \,|\, T M_T \rangle \langle \tfrac{1}{2}\tfrac{1}{2} \tau_f \alpha \,|\, T M_T \rangle N_i N_f (4\pi)^{3/2} i^L$$
$$\times \hat{L}^{\frac{1}{2}} \int r^2 \, dr \, j_0(Qr) V^{c}_{ST}(r) \int r_1^2 \, dr_1 \, j_L(Qr_1) R_{l_2 j_2}(r_1) R_{l_1 j_1}(r_1)$$
$$\times \langle l_2 m_{l_2} \,|\, Y_{L0}(\Omega_1) \,|\, l_1 m_{l_1} \rangle \langle \tfrac{1}{2}\tfrac{1}{2} \nu_i \mu_1 \,|\, S M_S \rangle \langle \tfrac{1}{2}\tfrac{1}{2} \nu_f \mu_2 \,|\, S M_S \rangle$$
$$\times (-)^{j_1 - m_1} \langle j_1 j_2 m_1 - m_2 \,|\, I - N \rangle \langle l_1 \tfrac{1}{2} m_{l_1} \mu_1 \,|\, j_1 m_1 \rangle \langle l_2 \tfrac{1}{2} m_{l_2} \mu_2 \,|\, j_2 m_2 \rangle . \tag{A2}$$

Using the Wigner–Eckart theorem and standard angular momentum algebra then yields the result equation (10a) given in the text.

Tensor Forces

The tensor force component of the t matrix can be recast as

$$t^{t} = \sum_{T} V^{t}_{T}(r) P^{T} (\tfrac{2}{3})^{\frac{1}{2}} \mathbf{T}_2(\boldsymbol{\sigma}_0, \boldsymbol{\sigma}_1) . \mathbf{C}_2(\Omega_{01}) , \tag{A3}$$

from which one may deduce that

$$\langle \tfrac{1}{2}\tfrac{1}{2}; S' M_{S'} \,|\, t^{t} \,|\, \tfrac{1}{2}\tfrac{1}{2}; S M_S \rangle = \sum_{Tq} V^{t}_{T}(r_{01}) \tfrac{2}{3} (8\pi)^{\frac{1}{2}} (-)^{q} \langle 12 M_S q \,|\, 1 M_{S'} \rangle$$
$$\times Y_{2-q}(\Omega_{01}) \delta_{S1} \delta_{SS'} . \tag{A4}$$

Again with the expansions of the bound state functions, recoupling to two-body spin and isospin functions and using the coordinate transformations, it is straightforward to develop equation (8) for a tensor force to

$$\mathcal{M}^{t}_{j_1 j_2} = \sum \hat{J}_B^{-\frac{1}{2}} \langle J_A I \nu_A N \,|\, J_B \nu_B \rangle N_i N_f \langle \tfrac{1}{2}\tfrac{1}{2} \tau_i \alpha \,|\, T M_T \rangle \langle \tfrac{1}{2}\tfrac{1}{2} \tau_f \alpha \,|\, T M_T \rangle$$
$$\times \langle \tfrac{1}{2}\tfrac{1}{2} \nu_i \mu_1 \,|\, 1 M_S \rangle \langle \tfrac{1}{2}\tfrac{1}{2} \nu_f \mu_2 \,|\, 1 M_{S'} \rangle \tfrac{2}{3} (8\pi)^{\frac{1}{2}} (-)^{q} \langle 12 M_S q \,|\, 1 M_{S'} \rangle$$
$$\times (-)^{j_1 - m_1} \langle j_1 j_2 m_1 - m_2 \,|\, I - N \rangle \langle l_1 \tfrac{1}{2} m_{l_1} \mu_1 \,|\, j_1 m_1 \rangle \langle l_2 \tfrac{1}{2} m_{l_2} \mu_2 \,|\, j_2 m_2 \rangle$$
$$\times \int d\boldsymbol{r} \exp(i \boldsymbol{Q} . \boldsymbol{r}) V^{t}_{T}(r) Y_{2-q}(\Omega)$$
$$\times \int d\boldsymbol{r}_1 \exp(i \boldsymbol{Q} . \boldsymbol{r}_1) R_{l_2 j_2}(r_1) R_{l_1 j_1}(r_1) Y^{*}_{l_2 m_{l_2}}(\Omega_1) Y_{l_1 m_{l_1}}(\Omega_1) . \tag{A5}$$

Multipole expansions of the 'plane' waves, use of the Wignert–Eckart theorem and standard angular momentum algebra then yield the result equation (10b).

Spin–Orbit Force

The spin–orbit force component of the t matrix may be handled most easily by using the cartesian coordinate expansion of

$$t^{\text{s.o.}} = \sum_T V_T^{\text{s.o.}}(r)\, P^T(-\mathrm{i}/\hbar)(\boldsymbol{r} \times \nabla)\cdot\boldsymbol{S}, \tag{A6}$$

whence

$$\begin{aligned} t^{\text{s.o.}} \exp(\mathrm{i}\,\boldsymbol{K}\cdot\boldsymbol{r})\,|\,SM_S\rangle \equiv \sum_T V_T^{\text{s.o.}}(r)\, P^T \exp(\mathrm{i}\,\boldsymbol{K}\cdot\boldsymbol{r})\{(yK_z - zK_y)(S_x/\hbar)\,|\,SM_S\rangle \\ +(zK_x - xK_z)(S_y/\hbar)\,|\,SM_S\rangle + (xK_y - yK_x)(S_z/\hbar)\,|\,SM_S\rangle\}. \end{aligned} \tag{A7}$$

Then with $\boldsymbol{Q}$ defining the z-axis, integrals of the form

$$I_{x,y,z} = \int \mathrm{d}\boldsymbol{r} \exp(\mathrm{i}\,\boldsymbol{Q}\cdot\boldsymbol{r})\, V_T^{\text{s.o.}}(r) \begin{pmatrix} x \\ y \\ z \end{pmatrix} \tag{A8}$$

result in the matrix elements, for which only I_z is non-vanishing. Thus the effective part of $t^{\text{s.o.}}$ in (A7) is, given $\boldsymbol{Q}$ as the z-axis and x–z as the scattering plane (whence $K_y = 0$),

$$t^{\text{s.o.}} \exp(\mathrm{i}\,\boldsymbol{K}\cdot\boldsymbol{r})\,|\,SM_S\rangle \sim \sum_T V_T^{\text{s.o.}}(r)\, P^T \exp(\mathrm{i}\,\boldsymbol{K}\cdot\boldsymbol{r})\, z\, K_x (S_y/\hbar)\,|\,SM_S\rangle, \tag{A9}$$

and the matrix elements (8) become

$$\begin{aligned} \mathscr{M}^{\text{s.o.}}_{j_1 j_2} = \sum (-)^{j_1 - m_1} &\langle j_1 j_2\, m_1 - m_2\,|\,I - N\rangle \hat{J}_{\text{B}}^{-\frac{1}{2}} \langle J_{\text{A}}\, I\nu_{\text{A}}\, N\,|\,J_{\text{B}}\,\nu_{\text{B}}\rangle N_{\text{i}}\, N_{\text{f}} \langle \tfrac{1}{2}\tfrac{1}{2}\tau_{\text{i}}\,\alpha\,|\,TM_T\rangle \\ &\times \langle \tfrac{1}{2}\tfrac{1}{2}\tau_{\text{f}}\,\alpha\,|\,TM_T\rangle \langle \tfrac{1}{2}\tfrac{1}{2}\nu_{\text{f}}\,\mu_2\,|\,S'M_{S'}\rangle \langle \tfrac{1}{2}\tfrac{1}{2}\nu_{\text{i}}\,\mu_1\,|\,SM_S\rangle \\ &\times \langle l_1\, \tfrac{1}{2} m_{l_1}\,\mu_1\,|\,j_1\, m_1\rangle \langle l_2\, \tfrac{1}{2} m_{l_2}\,\mu_2\,|\,j_2\, m_2\rangle K_{\text{i}}(x) \langle S'M_{S'}\,|\,S_y/\hbar\,|\,SM_S\rangle \\ &\times \int \mathrm{d}\boldsymbol{r}_0 \int \mathrm{d}\boldsymbol{r}_1 \exp(-\mathrm{i}\,\boldsymbol{K}_{\text{f}}\cdot\boldsymbol{r}_0)\, R_{l_2 j_2}(r_1)\, \mathrm{Y}^*_{l_2 m_{l_2}}(\Omega_1) \\ &\times r_{01} \cos\theta_{01}\, V_T^{\text{s.o.}}(r_{01}) \exp(\mathrm{i}\,\boldsymbol{K}_{\text{i}}\cdot\boldsymbol{r}_{01}) \exp(\mathrm{i}\,\boldsymbol{K}_{\text{i}}\cdot\boldsymbol{r}_1)\, R_{l_1 j_1}(r_1)\, \mathrm{Y}_{l_1 m_{l_1}}(\Omega_1). \end{aligned}$$

Transforming the variables and using

$$\begin{aligned} \langle S'M_{S'}\,|\,S_y/\hbar\,|\,SM_S\rangle &\equiv \langle S'M_{S'}\,|\,\mathrm{i}\sqrt{\tfrac{1}{2}}\,(S_+ + S_-)/\hbar\,|\,SM_S\rangle \\ &\equiv \delta_{SS'}\,\delta_{S1} \sum_\xi |\,\xi\,|\,\mathrm{i}\langle 11 M_S\,\xi\,|\,1M_{S'}\rangle \end{aligned}$$

then yields

$$\begin{aligned} \mathscr{M}^{\text{s.o.}}_{j_1 j_2} = \sum \hat{J}_{\text{B}}^{-\frac{1}{2}} &\langle J_{\text{A}}\, I\nu_{\text{A}}\, N\,|\,J_{\text{B}}\,\nu_{\text{B}}\rangle \langle \tfrac{1}{2}\tfrac{1}{2}\tau_{\text{i}}\,\alpha\,|\,TM_T\rangle \\ &\times \langle \tfrac{1}{2}\tfrac{1}{2}\tau_{\text{f}}\,\alpha\,|\,TM_T\rangle \langle \tfrac{1}{2}\tfrac{1}{2}\nu_{\text{i}}\,\mu_1\,|\,1M_S\rangle \langle \tfrac{1}{2}\tfrac{1}{2}\nu_{\text{f}}\,\mu_2\,|\,1M_{S'}\rangle \langle 11 M_S\,\xi\,|\,1M_{S'}\rangle \mathrm{i}\,|\,\xi\,|\,K_{\text{i}}(x) \\ &\times (-)^{j_1 - m_1} \langle j_1 j_2\, m_1 - m_2\,|\,I - N\rangle \langle l_1\, \tfrac{1}{2} m_{l_1}\,\mu_1\,|\,j_1\, m_1\rangle \langle l_2\, \tfrac{1}{2} m_{l_2}\,\mu_2\,|\,j_2\, m_2\rangle \\ &\times \int \mathrm{d}\boldsymbol{r} \exp(\mathrm{i}\,\boldsymbol{Q}\cdot\boldsymbol{r})\, V_T^{\text{s.o.}}(r)\, r\cos\theta \\ &\times \int \mathrm{d}\boldsymbol{r}_1 \exp(\mathrm{i}\,\boldsymbol{Q}\cdot\boldsymbol{r}_1)\, R_{l_2 j_2}(r_1)\, R_{l_1 j_1}(r_1)\, \mathrm{Y}^*_{l_2 m_{l_2}}(\Omega_1)\, \mathrm{Y}_{l_1 m_{l_1}}(\Omega_1). \end{aligned}$$

Standard algebra then yields equation (10c) when, for high energies and small q values, K_i and K_f are equal and give

$$K_i(x) = K_f(x) = (K_i^2 - \tfrac{1}{4}Q^2)^{\frac{1}{2}}.$$

With this last condition, the results quoted would also be obtained if the more symmetric form

$$t^{s.o.} = \sum_T \tfrac{1}{2}P^T\{V_T^{s.o.}(r)(\boldsymbol{L}.\boldsymbol{S}/\hbar^2) + (\boldsymbol{L}.\boldsymbol{S}/\hbar^2)V_T^{s.o.}(r)\}$$

was to be used in the development.

Manuscript received 29 October, accepted 25 November 1982